




## Enhancing Performance and Optimizing Energy Utilization and Voltage Regulation in Hybrid Wind-Solar Pumping Systems



Mebrouk Mennad<sup>\*</sup>, Bentaallah Abderrahim<sup>\*</sup>, Djeriri Youcef<sup>\*</sup>

ICEPS Laboratory, Engineer Sciences Faculty, Djillali Liabès University, Sidi Bel-Abbès 22000, Algeria

Corresponding Author Email: [mabroukmenad@gmail.com](mailto:mabroukmenad@gmail.com)

Copyright: ©2024 The authors. This article is published by IETA and is licensed under the CC BY 4.0 license (<http://creativecommons.org/licenses/by/4.0/>).

<https://doi.org/10.18280/jesa.570411>

### ABSTRACT

**Received:** 5 May 2024

**Revised:** 17 July 2024

**Accepted:** 5 August 2024

**Available online:** 27 August 2024

#### Keywords:

*wind turbines, photovoltaic systems, induction motor, saturation magnetic, pumping systems, sliding mode control, fuzzy logic control*

The integration of renewable energy sources (RESs), is a workable way to meet operational demands and boosting industrial activities' efficiency, sustainability, reduce and environmental effect, in particular, in the field of pumping systems. This study looks into the effective dynamic integration of wind turbines and photovoltaic (PV) systems to drive an induction motor (IM) under varying environmental conditions. Results show that the integrated system's power output grows in direct proportion to the intensity of solar radiation and wind speed, which enables the IM to operate more efficiently and accelerate. The study's cutting-edge control systems, in particular, operate very well by utilising sliding mode control (SMC) to keep the rotor flux within safe operating limits, hence avoiding magnetic saturation and possible motor failures. The study also emphasises how well the reference speed adjustment (RSA) system works to stabilise the DC link voltage with fuzzy logic approaches, guaranteeing that the IM's generated power is used as efficiently as possible while avoiding undesired fluctuations.

## 1. INTRODUCTION

The increase in energy request due to industrial development and modernization is projected to rise by 56.0% over the next three decades, this substantial surge in energy demand will inevitably have environmental repercussions. addressing this increased energy request through modern energy solutions, such as RESs, can reliably power supply, and affordable electricity generation and reducing the reliance on conventional energy sources and mitigating their environmental impacts. RESs play a crucial role not only in industrialization and modernization, but also for water pumping applications. By harnessing renewable energy for water pumping, it is possible to achieve sustainable water management while reducing carbon emissions and environmental degradation associated with the use of fossil fuels [1-6].

Unlike conventional energy sources, individual renewable energy systems like wind turbines and solar panels cannot reliably meet continuous load demands. Therefore, hybrid energy systems, which harness two or more renewable resources, have emerged as more reliable and carbon dioxide-free alternatives [3, 6]. Therefore, hybrid renewable energy systems (HRES) present an attractive solution for standalone power generation. They offer promising prospects for supplying reliable power while also promoting environmental cleanliness. HRES can play a crucial role in transitioning island nations and other remote regions away from costly and environmentally harmful fossil fuels towards sustainable and affordable energy sources.

### 1.1 Literature review

Bhayo et al. [3] discussed the analysis and optimization of a HRES for a housing unit, utilizing rainfall harvesting and a PV-battery system. The study aims to minimize component oversizing and ensure reliable power supply management using the particle swarm optimization technique (PSO). The study demonstrates that integrating rainfall harvesting with a PV-battery system can achieve environmentally appropriate, reliable, and cost-effective power generation. The proposed system reduces dependency on battery storage, which is the most expensive component with a short lifespan in integrated renewable systems. Harndi et al. [4] aimed to enhance optimization techniques for maximizing the efficiency of a PV pumping system, The results showed the superior performance of sliding-neuron control in reducing chattering and deviation from the reference. Abuashour et al. [5] presented a hybrid system (HS) consists of a wind turbine connected to a self-excited induction generator, a PV array is integrated with a DC-DC converter, inverter, and LC filter. The performance of the HS was evaluated under varying conditions. The results indicate that the system can operate effectively over a wide range of solar intensity levels and IM loading conditions. Obaid et al. [6] presented the design of a hybrid power system for water pumping applications. It was utilized two main RESs: solar PV panels and wind turbines. The design took into account variations in weather conditions, such as humidity, wind speed, and temperature, as these factors impact the performance of both wind turbines (wind speed) and solar panels (solar irradiance). A neural network was employed for weather forecasting based on five years of historical data for

temperature, wind speed, and humidity in Sharjah. A robust control method for a two-stage water pumping system was suggested by Massaqa et al. [7], the maximum power point (MPP) was tracked in the first stage using a boost converter controlled using a fuzzy logic technique that had a configurable step size. a nonlinear predictive controller was employed in the second stage, which consists of a three-phase inverter controlling the DC-link voltage and the rotor speed of the IM, in comparison to the old system (P&O algorithm for MPPT and field-oriented control (FOC) control of the IM), the results showed that the advanced control approaches give superior performance, such as fast tracking of the MPP and stable output power. An Analytical MPPT Control (AMPPTC) for a PV water pumping system based on an IM was presented in the study [8]. The AMPPTC system shows rapid dynamic performance and minimal overshoot with the water pumping system. Additionally, the AMPPTC scheme offers robust absolute state stability under variations in solar irradiation/operational parameters, optimizing system stability while ensuring regulation of the DC-link voltage. Hosseinzadeh and Heydari [9] suggested using a Linear Quadratic Regulator (LQR) for controlling a standalone single-phase PV pumping system, utilizing a permanent magnet synchronous motor (PMSM). The reference speed is determined using the P&O MPPT method. The system behavior was evaluated under various environmental conditions. Total harmonic distortion (THD) of the stator currents was assessed, showing that the proposed control system provides low harmonic distortion. An adaptive neuro-fuzzy inference system (ANFIS) was adopted in the study [10] for controlling a PV pumping system. Additionally, the performance of the vector SMC integration with a neural network was evaluated to improve the performance of the pumping system, which is based on IM. The results demonstrated the success of the proposed control method under varying load torque conditions. Add to that, the use of a neural network also contributed to reducing the phenomenon of chatter that results from the use of a switching function in a SMC. This chatter phenomenon may cause the application of high-frequency control signals, causing significant distortions in the electrical signals or in the electromagnetic torque signal of the IM. But with the use of a neural network to adjust control signals, this can be reduced, as the researchers used two neural networks in parallel to accomplish the equivalent command.

### 1.2 Problem statements

From these reference studies, the following points can be concluded:

Focus on improving energy efficiency and dynamic control of pumping systems based on RESs, through the use of advanced control techniques such as radial control, fuzzy control, and nonlinear predictive control systems. The focus is on reducing noise and performance overruns as well as enhancing the overall stability of the system, especially under input fluctuations such as solar radiation intensity. Studies indicate the possibility of operating the systems in diverse conditions and under different loads, demonstrating the need of flexibility and adaptability of the control systems to meet different operating requirements.

Some of the shortcomings in the published articles include not evaluating the voltage value at the dc-link with changes in environmental conditions and not evaluating the motor's

performance when there is a change in the rotor resistance value, or operating at a constant speed due to the presence of batteries within the pumping system, knowing that the presence of batteries increases the cost of the system. With most research dealing with the issue of control focusing on PV systems only, it is noted that there is a shortage of articles that address the issue of controlling a HS without batteries.

Managing a battery-free HS poses specific challenges:

1. It is challenging to maintain an immediate supply and demand balance in the absence of an energy storage buffer.
2. advanced control algorithms are needed to match available power to the load dynamically.
3. Because RESs, like wind and solar are erratic, it is difficult to keep the power supply steady.
4. it may be need to connecting the system to grid in order to absorb excess energy or provide backup during shortages.

This research aims to study and simulate a generation HS (wind-solar) feeding a 3-ph IM work as a pump. Fuzzy logic controller (FLC) will be used to determine the reference speed of the IM in order to fully exploit the energy provided by the generation HS and maintain the DC link voltage within allowed values.

The research also proposes a control method based on the SMC to regulate the IM speed and rotor magnetic flux to overcome the state of magnetic saturation that can occur with using of the traditional FOC method when changing the rotor coil resistance value of the IM.

## 2. CONFIGURATION OF PROPOSED SYSTEM

Figure 1 shows the structure of the proposed system, which consists of PV panels connected with a boost converter controlled in order to achieve the maximum power of the PV panels and a permanent magnetic synchronization generator (PMSG) driven by a wind turbine. The PMSG is connected with a three-phase rectifier controlled using the FOC method in order to regulate the speed on the reference value determined using the maximum power point tracking (MPPT) system related to wind turbine based on tip speed ratio (TSR) method [11]. The generation HS feeds an IM operating as a pump for water. The IM is driven by a voltage source inverter (VSI) controlled using the FOC method in order to regulate speed, whose reference value is determined according to the power provided by the generation HS using the FLC.

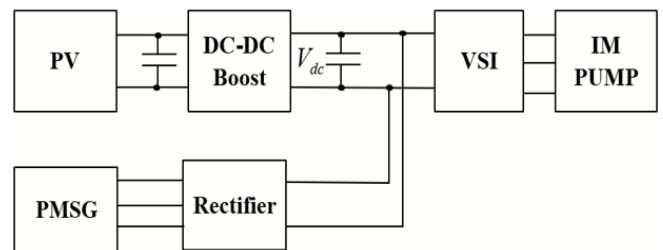


Figure 1. The block diagram of the proposed system

The FLC adjusts the reference speed of the IM, ensuring that the IM's power matches the power provided by the HS. It works to increase the IM speed (which means increasing the IM power) when there is an increase in the power provided by the HS, and vice versa, while maintaining the permissible limits of the dc-link voltage.

### 3. MATHEMATICAL SYSTEM MODEL

#### 3.1 PV system model

PV systems harness energy from the sun through PV cells, converting sunlight directly into electricity. It consists of PV panels connected with boost converter controlled in order to achieve the maximum power of the PV panels. PV cells, which are composed of semiconductor materials, are the main component of the PV panel [7, 12]. The PV cell is commonly represented by the electrical circuit model shown in Figure 2.

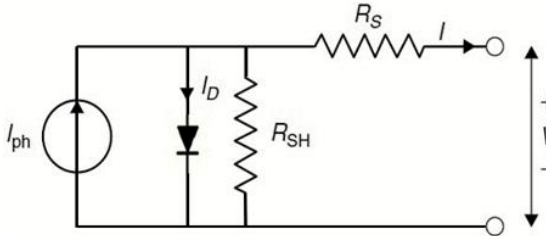


**Figure 2.** Equivalent circuit for a single PV cell model

The mathematical model of PV cell is given as:

$$I = [I_{sc} + k_I(T_c - T_{ref})] \frac{G}{1000} - I_D - \frac{V + IR_S}{R_{sh}} \quad (1)$$

$$I_D = I_s \left\{ \exp \left[ \frac{e(V + IR_S)}{N_s k A T_c} \right] - 1 \right\} \quad (2)$$

$$I_s = \left( \frac{I_{sc}}{\exp \left\{ \frac{eV_{oc}}{N_s k A T_c} - 1 \right\}} \right) \left( \frac{T_c}{T_{ref}} \right)^3 \exp \left\{ \frac{e E_g}{k A} \left[ \frac{1}{T_{ref}} - \frac{1}{T_c} \right] \right\} \quad (3)$$

The boost converter model used in this paper is depicted in Figure 3, its dynamic model is provided below.

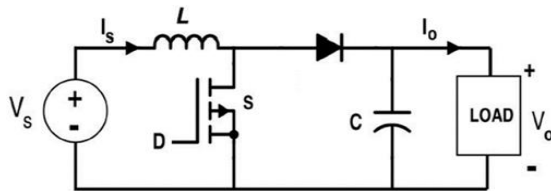


**Figure 3.** The structure of the boost converter

$$\frac{V_o}{V_s} = \frac{1}{1 - D} \quad (4)$$

$$\frac{dI_s}{dt} = \frac{-(1 - D)V_o + V_s}{L} \quad (5)$$

$$\frac{dV_o}{dt} = \frac{(1 - D)I_s - I_o}{C} \quad (6)$$

#### 3.2 Wind-PMSG model

The variable speed wind energy generating system (VS-WEGS), which has several advantages that make it a competitive option for the generation of sustainable green energy, is one of the renewable energy technologies that is growing the fastest. The usage of PMSG with high power density and simplicity of implementation allows VS-WEGS to

achieve great efficiency. It also lessens the requirement for intricate mechanical parts, which raises system dependability and lowers maintenance expenses. Better wind energy utilisation and increased annual energy production are made possible by VS-WEGS's flexible operation. Since VS-WEGS emits no harmful emissions, it contributes to environmental preservation and the slowing of climate change. PMSG's are also very effective at low wind speeds, which makes them ideal for a variety of wind energy applications. Furthermore, Because the PMSG does not have brushes or slipping rings, wind-PMSG systems have a number of benefits. These include high efficiency, low maintenance requirements. Add to that, the generator's use of permanent magnets removes the requirement for a separate excitation mechanism, streamlining the overall design [13-15].

Three factors affect a wind turbine: rotational speed, pitch angle, and wind speed. The torque applied to the generator mechanically is the output signal that results. The following formula is used to calculate the kinetic energy carried by wind currents:

$$P_{wind} = 0.5 \rho \pi R^2 V^3 \quad (7)$$

The following formula determines how much mechanical power the turbine can extract from the wind's motion:

$$P_t = P_{wind} C_p(\beta, \lambda) \quad (8)$$

$$C_p = c_1 \left( c_2 \left( \frac{1}{\lambda + 0.08\beta} - \frac{0.035}{\beta^3 + 1} \right) - c_3 \beta - c_4 \right) e^{-c_5 \left( \frac{1}{\lambda + 0.08\beta} - \frac{0.035}{\beta^3 + 1} \right)} + c_6 \lambda \quad (9)$$

$$\lambda = \frac{R \omega_m}{V} \quad (10)$$

The torque furnished by the wind turbine can be computed using the equation:

$$T_{mech} = \frac{P_t}{\omega_m} \quad (11)$$

The following form represents the dynamical model of a PMSG in  $d, q$  frame [14, 15]:

$$L_{gd} \frac{di_{gd}}{dt} - \omega_g L_{gq} i_{gq} + R_g i_{gd} = V_{gd} \quad (12)$$

$$L_{gq} \frac{di_{gq}}{dt} + \omega_g L_{gd} i_{gd} + \omega_g \Phi_m + R_g i_{gq} = V_{gq} \quad (13)$$

$$\frac{d\omega_g}{dt} = \frac{1.5 P_g^2 \Phi_m i_{gq}}{J_g} - \frac{P_g T_{mech}}{J_g} - \frac{f_g}{J_g} \omega_g \quad (14)$$

#### 3.3 IM model

The mathematical model for a three-phase IM in  $d, q$  frame is given as follows [16, 17]:

$$\frac{di_{sd}}{dt} = -a_5 i_{sd} + \omega_k i_{sq} + a_3 \Phi_{rd} + a_4 \omega \Phi_{rq} + b v_{sd} \quad (15)$$

$$\frac{di_{sq}}{dt} = -\omega_k i_{sd} - a_5 i_{sq} - a_4 \omega \Phi_{rd} + a_3 r_q + b v_{sq} \quad (16)$$



#### 4.3.1 FOC control of IM using Proportional-integral controllers (PIC)

PIC are considered one of the easiest and simplest controllers used with electric motors, electrical machines, and control systems in general, although they have some disadvantages, as they are sensitive to changing system parameters and are affected by the mathematical uncertainty

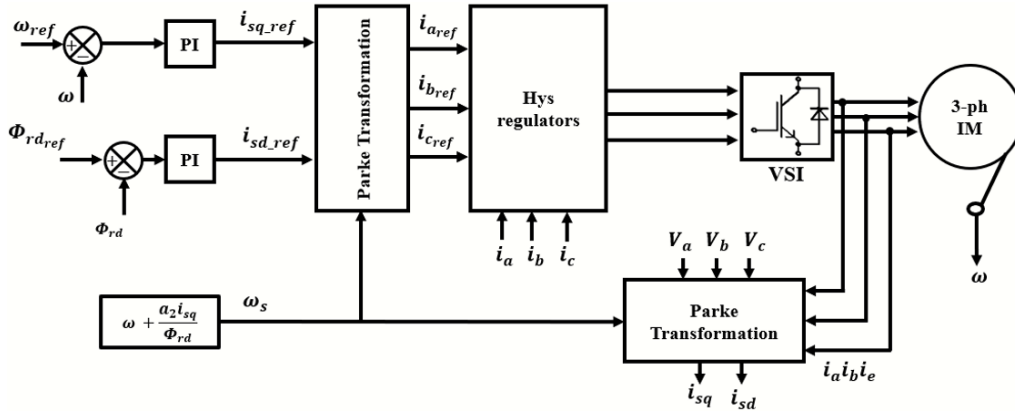


Figure 6. Block diagram of the traditional FOC system

#### 4.3.2 FOC control of IM using SMC technology

The SMC is a control technology for systems with a variable structure. It was first studied in the former Soviet Union. It is characterized by its robustness, its ability to resist changes in machine parameters, and its relative ease of application. This methodology is based on Lyapunov's law to ensure the stability of the system. This algorithm includes two stages: The first stage is the attraction stage, where the controlled state variable is attracted towards the sliding surface. The second stage is the sliding stage, where the variable slides towards the equilibrium point, and therefore the final control law according to this algorithm includes two basic terms: the first term expresses the equivalent effort, and the second term expresses the attraction effort, as the following equation shows [26-28]:

$$v = v_{eq} + v_{att} \quad (26)$$

$V_{eq}$ : Equivalent term is the effort that maintains regulated state variables on the sliding surface.

$V_{att}$ : The attraction term is the effort that forces the regulated state variable to move towards the sliding surface.

In order to get at the final control law, the design of an SMC involves the suitable selection of both the sliding surface and the law of attraction. The sliding surface should be chosen according to the control requirements, including minimizing static error, improving transient performance, and not complicating the control system. As for choosing the law of attraction, it is subject to criteria related to the phenomenon of chatter, response speed, and flexibility in the control system.

The sliding surface function can be expressed as follows to control speed:

$$S_\omega = \omega_{ref} - \omega \quad (27)$$

By differentiating the relationship (27) and substituting the relationship (19), we find:

$$\dot{S}_\omega = \dot{\omega}_{ref} - (P/J)(G\Phi_{rd}i_{sq}) + (f/J)\omega \quad (28)$$

of the system. Figure 6 shows the block diagram of a traditional FOC drive system, it consists of two loops, the speed and rotor flux are regulated in the outer loop using PIC, and the currents are regulated in the inner loop using hysteresis (Hys) regulators that generate the pulses necessary for the operation of the inverter feeding the IM.

where,  $G = PL_m/L_r$ .

In order to force the speed to move towards the sliding surface, a law of attraction can be chosen as follows:

$$\dot{S}_\omega = -K_1 \text{sig}(S_\omega) - Q_1(S_\omega) \quad (29)$$

By making an equality between the two relations (28) and (29), we find

$$i_{sqref} = (\dot{\omega}_{ref} + \omega f/J + K_1 \text{sig}(S_\omega) + Q_1(S_\omega)) / ((PG/J)\Phi_{rd}) \quad (30)$$

In order to regulate the flux  $\Phi_{rd}$ , we first impose the following slip surface function:

$$S_d = \Phi_{rd-ref} - \Phi_{rd} \quad (31)$$

By differentiating the relationship (31) and substituting the relationship (17), we find:

$$\dot{S}_d = \dot{\Phi}_{rd-ref} - a_2 i_{sd} + a_1 \Phi_{rd} - (\omega_k - \omega)\Phi_{rq} \quad (32)$$

A law of attraction can be chosen as follows to regulate the flux  $\Phi_{rd}$ :

$$\dot{S}_d = -K_2 \text{sig}(S_d) - Q_2(S_d) \quad (33)$$

By equating relations (32) and (33), we find:

$$i_{sd-ref} = (\dot{\Phi}_{rd-ref} + a_1 \Phi_{rd} - (\omega_k - \omega)\Phi_{rq} + K_2 \text{sig}(S_d) + Q_2(S_d)) / a_2 \quad (34)$$

As previously noted, when using conventional PI controllers, to obtain the value of  $\omega_k$ , the relationship (12) is relied upon, which includes online variable parameters, but the control system will still depend on the nominal values of the IM, causes entering a state of magnetic saturation and the inability of the system to achieving the correct orientation of the magnetic flux vector since there is no regulation of the flux

$\Phi_{rq}$  because the value of  $\omega_k$  is obtained in an open loop system.

Therefore, we will adopt here the regulation of the component of the flux  $\Phi_{rq}$  using a special control loop to obtain the value of  $\omega_k$  according to the following:

We first assume the following sliding surface function:

$$S_q = \Phi_{rq-ref} - \Phi_{rq} \quad (35)$$

By differentiating the relationship (35) and substituting the relationship (18), we find:

$$\dot{S}_q = \dot{\Phi}_{rq-ref} - a_2 i_{sq} + (\omega_k - \omega) \Phi_{rd} + a_1 \Phi_{rq} \quad (36)$$

A law of attraction can be chosen as follows to regulate the flux  $\Phi_{rq}$ :

$$\dot{S}_q = -K_3 sig(S_q) - Q_3(S_q) \quad (37)$$

By equating relations (36) and (37), we find:

$$\omega_k = (a_2 i_{sq} - a_1 \Phi_{rq} - K_3 sig(S_q) - Q_3(S_q)) / \Phi_{rd} + \omega \quad (38)$$

where,  $Q_i, K_i$  constants whose values must be chosen in a way that fulfills Lyapunov's conditions for stability.

Figure 7 shows the block diagram of the FOC drive system using SMC with Hys regulators.

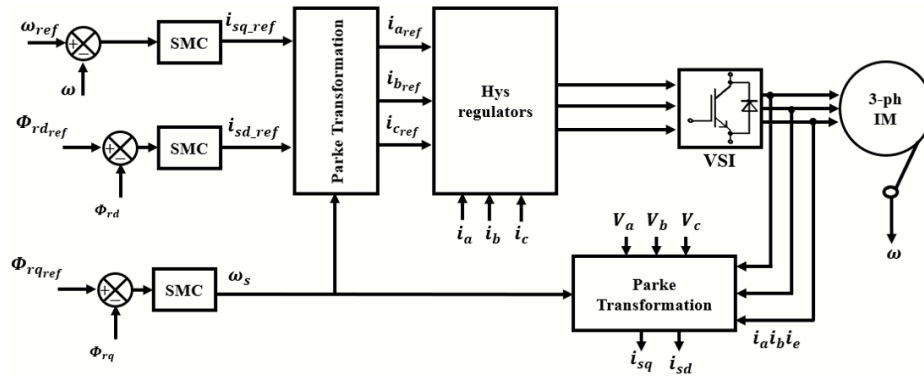


Figure 7. Block diagram of the advanced FOC system

#### 4.4 RSA system of IM drive

RSA system in this context refers to a control system that optimizes the operation of various components within the REHS to ensure efficient energy utilization and system stability. RSA system for the IM drive within the REHS plays a significant role in ensuring the system's reliable and efficient operation, as well as its integration with the broader energy infrastructure.

The RSA of the IM drive within the REHS can be vital for several reasons:

1. REHS often have varying energy demands based on factors like weather conditions; by adjusting the reference speed of the IM drive, the system can better match the energy output to the current demand, ensuring optimal operation.

2. Operating the IM drive at its most efficient speed can help minimize energy losses and increase overall system efficiency,

which is crucial for RES, aiming for sustainability and cost-effectiveness.

In this research, a FLC was developed to adjust the reference speed, which takes into account the power provided by the hybrid generation system and the voltage value of the dc-link, ensuring full use of the power provided and keeping the voltage value stable within the permissible limits.

The Figure 8 illustrates the structure of a reference speed control system. Five membership function sets are used for both input and output signals of the FLC with triangular membership functions. The input signals are  $dV_{dc}$  and  $dPower$  and the output signal is  $d\omega_{ref}$ , where:  $dV_{dc} = V_{dc}(k) - V_{dc}(k-1)$ ,  $dPower = power(k) - Power(k-1)$ ,  $d\omega_{ref} = \omega_{ref}(k) - \omega_{ref}(k-1)$ . The rules base of FLC is shown in Table 1.

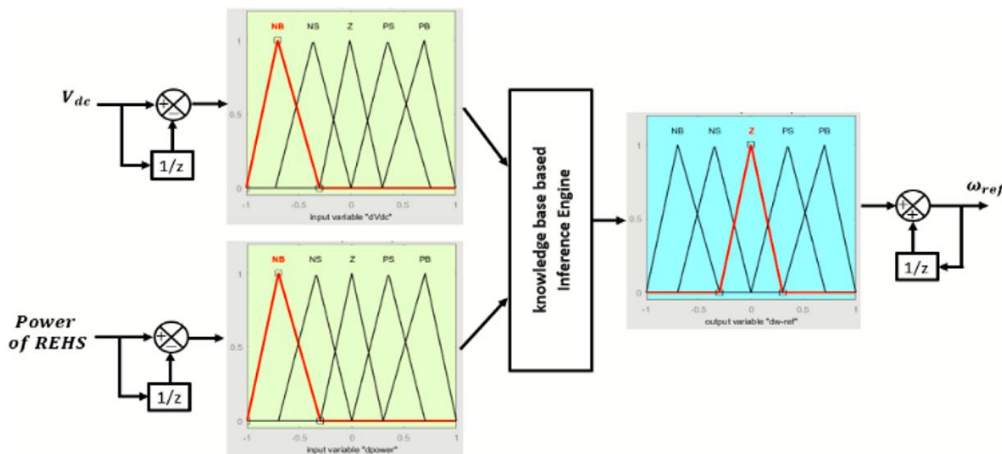


Figure 8. The structure of RSA based on FLC

**Table 1.** Rules base of fuzzy controller

$dPower$	$dV_{dc}$	NB	NS	Z	PS	PB
NB	NB	NB	NS	NS	Z	Z
NS	NB	NB	NS	Z	Z	PS
Z	NS	NS	NS	Z	PS	PS
PS	NS	Z	Z	Z	PS	PB
PB	Z	Z	PS	PS	PS	PB

**5. SIMULATION RESULTS AND DISCUSSION**

In the proposed model, the IM nominal power is 15kw, and the PMSG nominal power is 6kw. The parameters of PV panels are shown in Table 2.

**Table 2.** The parameters of used panel

Parameters	Value
Parallel strings	3
Series-connected modules per string	25
Maximum power	152.4 w
Open circuit voltage $V_{oc}$	21.2 v
Voltage at maximum power point $V_{mp}$	17.23 v
Short-circuit current $I_{sc}$	9.27 A
Current at maximum power point $I_{mp}$	8.85 A
Maximum power all panels	11.4 kw

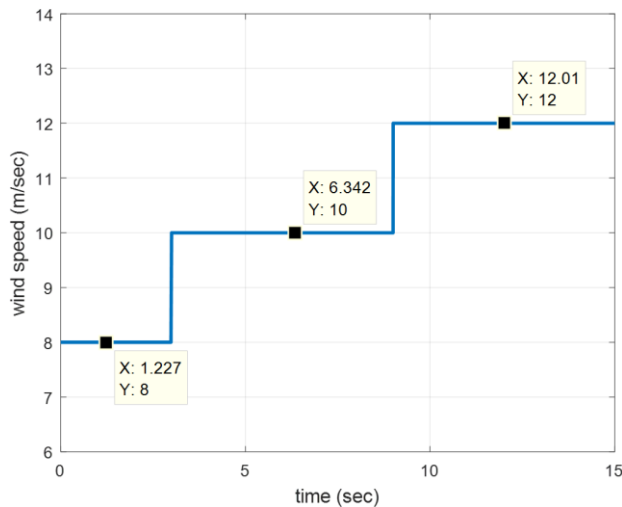


**Figure 9.** The changes in wind speed

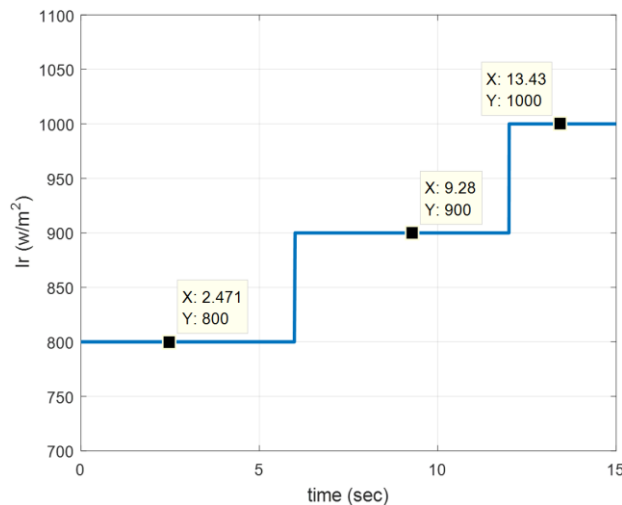


**Figure 10.** The changes in irradiation

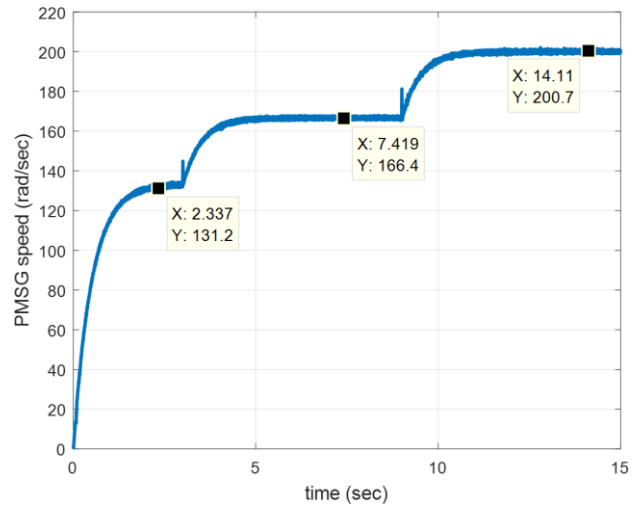


**Figure 11.** The rotational speed of PMSG

Figure 9 shows the changes in wind speed, where it was assumed that the wind speed would be 8m/s during the period 0-3sec, 10m/s during the period 3-9sec, and 12m/s during the period 9-15sec. Figure 10 shows the changes in Irradiation, where It was assumed that the Irradiation would be 800w/m<sup>2</sup> during the period 0-6sec, 900w/m<sup>2</sup> during the period 6-12sec, and 1000w/m<sup>2</sup> during the period 12-15 sec. It must also be taken into account that an increase in the rotor resistance value of 30% was assumed.

Figure 11 shows the changes in the rotational speed of PMSG, it is noted that the PMSG speed increases in proportion to the wind speed in order to track the point of maximum power that PMSG can provide.

As the wind speed increases and the solar radiation increases, the energy supplied increases, and thus the pump rotation speed increases, as shown in Figure 12, which shows the response of the two driving systems to regulating IM speed. It can be seen that both driving systems achieve high dynamic performance, in terms of accuracy and fast tracking the reference speed imposed by the RSA system. However, from Figure 13, it can be noted that the advanced drive system is superior in its ability to maintain the value of the rotor flux within the nominal value (1wb) despite the increase in the value of the rotor resistance, this contributes to preventing the occurrence of magnetic saturation, which contributes to reducing the malfunctions that can occur in the IM.

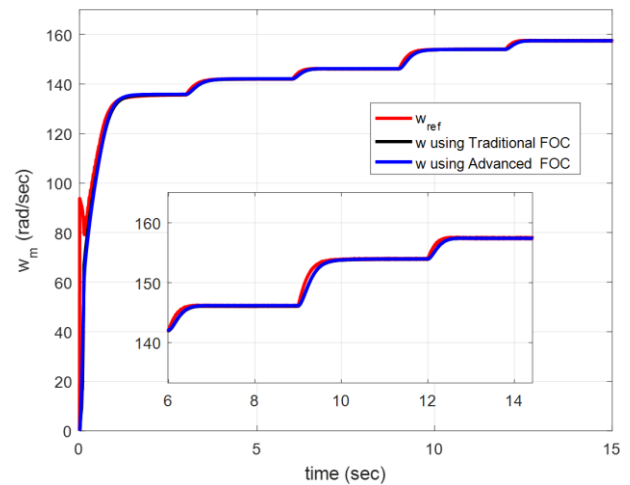


**Figure 12.** Responses of IM speed control systems

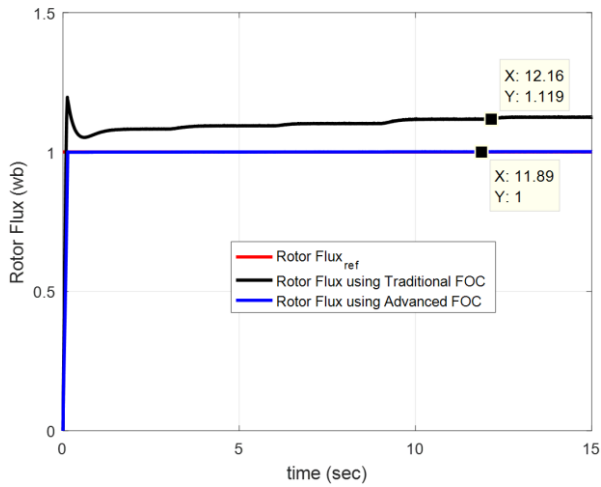


Figure 13. Responses of rotor flux control systems

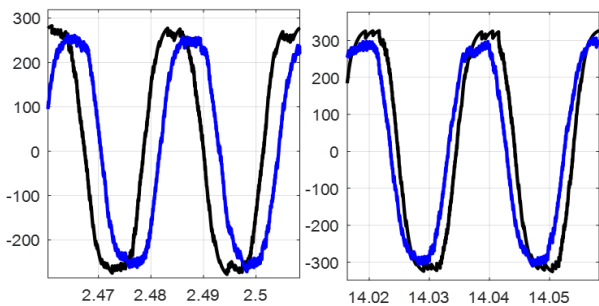
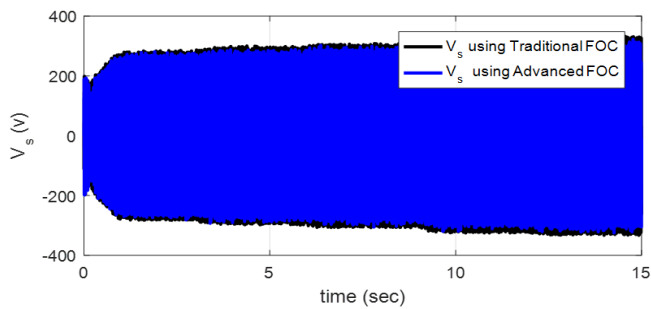


Figure 14. The voltage wave applied on the IM stator

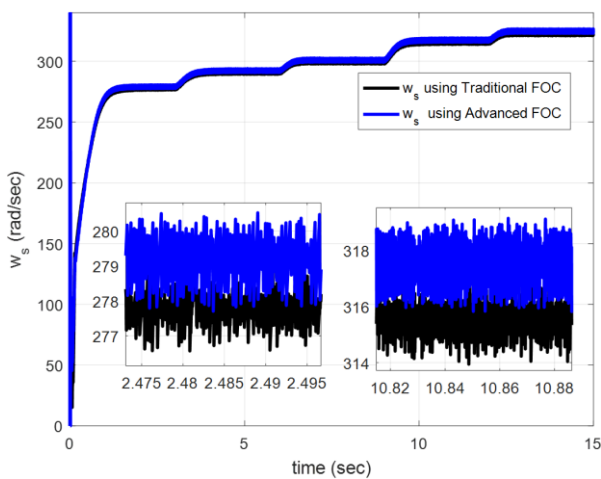


Figure 15. The voltage frequency applied on the IM stator

The phenomenon of magnetic saturation can be explained by the fact that the voltage to frequency ratio is greater when using a traditional FOC system. Figures 14 show the two voltage waves applied for both systems, and Figure 15 shows

the electrical frequency. It is clear that the applied voltage in the case of a traditional FOC system is greater, and correspondingly, the electrical frequency is lower compared to the use of an advanced FOC system.

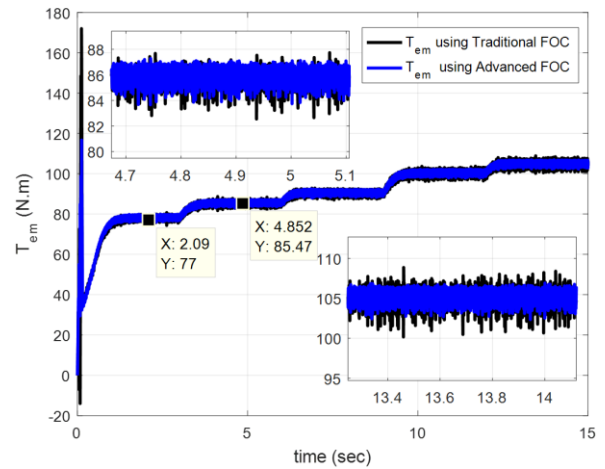


Figure 16. The electromagnetic torque of IM

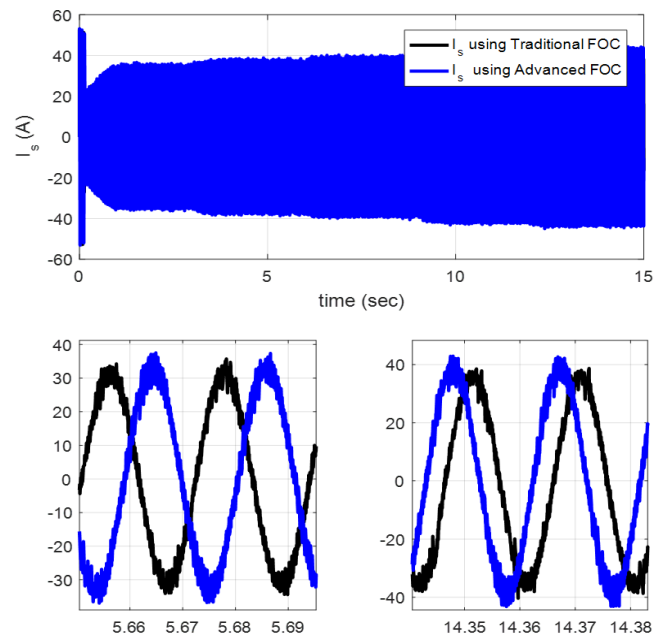


Figure 17. The current wave drawn by the IM stator

An increase in IM speed will be accompanied by an increase in torque based on relationship 21, and thus an increase in the current drawn by the IM, as shown in Figures 16 and 17, respectively. Obviously in Figure 16, torque ripples when using the advanced FOC system are less. It is noted from Figure 17 that the value of the current is slightly larger when using the advanced FOC system, because the voltage applied in this case is less compared to the traditional FOC system, as the IM in both cases needs the same value of electrical power in order to provide the ability to rotate at the same speed and generate the same torque value.

Stability in the rotational speed reflects the accuracy and effectiveness of the RSA system work, which works to adjust the DC link voltage and fully utilize the generated energy form PV system and PMSG. It can be seen from Figure 18 that the DC link voltage remains at its nominal value without any unwanted excesses. The presence of a difference between the power supplied and the power consumed will cause current to



flow through the DC link capacitor, and thus increase the voltage to high and inappropriate values, while it is noted that the voltage value here is stable, which indicates the effectiveness of the proposed system efficiency.

Figure 19 shows the power values for each PV system and the wind generation system, and the power consumed in the IM. It can be noted that the power provided by PV panels increases with increasing solar radiation and reaches its nominal value (11.38kw) when the radiation value is 1000w/m<sup>2</sup>, On the other hand, the power provided by the PMSG reaches its nominal value (6kw) when a wind speed is equal to 12m/sec. It is noted that all the energy provided by the PV panels and the wind generator is converted into mechanical energy on the IM shaft, taking into account the value of the losses consumed in it in addition to the losses present in the electronic transformers.

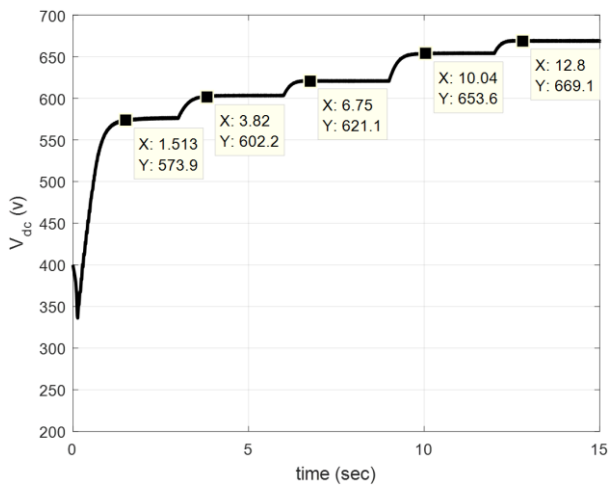


Figure 18. The DC link voltage

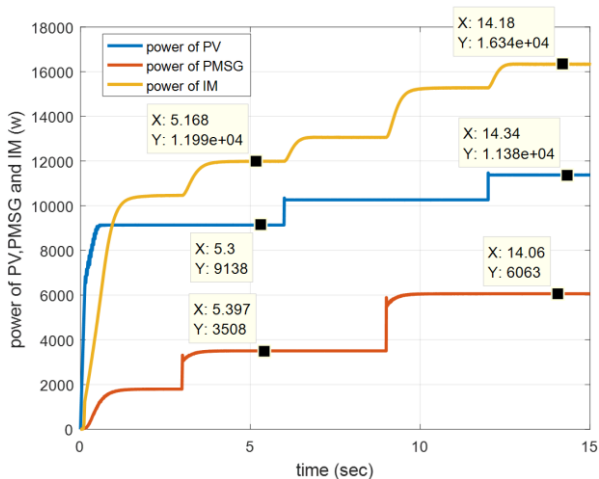


Figure 19. The power for each PV system, PMSG, and IM

## 6. CONCLUSIONS

This study explored the dynamic integration of PV systems and wind turbines, specifically focusing on their capability to efficiently drive an IM under variable environmental conditions. The research findings are grounded in detailed analysis across multiple operational scenarios.

The study's key findings are illustrated in the response of IM's rotational speed to changes in power input from both the

wind and solar systems. As wind speed and solar radiation intensify, the power output from both systems increases correspondingly, allowing the IM to accelerate to meet the required operational speeds. Notably, the advanced drive system showcased superior performance by maintaining rotor flux within safe operational limits, thus preventing magnetic saturation and potential IM malfunctions. This feature highlights the significance of advanced control systems in managing the variable nature of RESs, efficiently.

Further, the stability in the rotational speed and DC link voltage reinforces the effectiveness of the RSA system. The RSA system's ability to stabilize the DC link voltage prevents undesirable fluctuations, ensuring that the IM operates within safe electrical thresholds. This was particularly evident from the data indicating that all generated power was optimally utilized by the IM.

Moreover, the study demonstrated that the integrated system not only meets the energy demands of the IM but does so with high efficiency and dynamic performance, adapting swiftly to changes in input conditions. This research underscores the potential of integrating RESs, with advanced control systems to enhance the performance and reliability of industrial motors.

## REFERENCES

- [1] Zhang, C., Wang, L., Li, H. (2020). Experiments and simulation on a late-model wind-motor hybrid pumping unit. *Energies*, 13(4): 994. <https://doi.org/10.3390/en13040994>
- [2] Nóbrega, J., Araújo, T. (2011). The wind energy apply to water pumping in isolated place. In *International Conference on Renewable Energies and Power Quality*, Las Palmas de Gran Canaria, Spain, pp. 894-898. <https://doi.org/10.24084/repqj09.488>
- [3] Bhayo, B.A., Al-Kayiem, H.H., Gilani, S.I., Ismail, F.B. (2020). Power management optimization of hybrid solar photovoltaic-battery integrated with pumped-hydro-storage system for standalone electricity generation. *Energy Conversion and Management*, 215: 112942. <https://doi.org/10.1016/j.enconman.2020.112942>
- [4] Harndi, H., Regaya, C.B., Zaafouri, A. (2020). A sliding-neural network control of induction-motor-pump supplied by photovoltaic generator. *Protection and Control of Modern Power Systems*, 5(1): 1-17. <https://doi.org/10.1186/s41601-019-0145-1>
- [5] Abuashour, M.I., Widyana, M.S., Sweidan, T.E.O., Momani, M.A. (2018). Modelling, simulations and operational performance of a stand-alone hybrid wind/PV energy system supplying induction motor for pumping applications. *International Journal of Engineering Systems Modelling and Simulation*, 10(1): 12-25. <https://doi.org/10.1504/IJESMS.2018.090237>
- [6] Obaid, W., Hamid, A.K., Ghenai, C. (2021). Solar/wind pumping system with forecasting in Sharjah, United Arab Emirates. *International Journal of Electrical and Computer Engineering*, 11(4): 2752-2759. <https://doi.org/10.11591/ijece.v11i4.pp2752-2759>
- [7] Massa, Z., Chbirik, G., Abounada, A., Brahmi, A., Ramzi, M. (2020). Control of photovoltaic water pumping system employing non-linear predictive control and fuzzy logic control. *International Review on Modelling and Simulations*, 13(6): 373-382.

- <https://doi.org/10.15866/iremos.v13i6.18615>
- [8] Shukla, S., Singh, B., Shaw, P., Al-Durra, A., El-Fouly, T.H., El-Saadany, E.F. (2021). A new analytical mppt-based induction motor drive for solar PV water pumping system with battery backup. *IEEE Transactions on Industrial Electronics*, 69(6): 5768-5781. <https://doi.org/10.1109/TIE.2021.3091929>
- [9] Hosseinzadeh, A., Heydari, H. (2022). Control of standalone single-stage photovoltaic pumping system using state feedback approach. In 2022 9th Iranian Conference on Renewable Energy & Distributed Generation (ICREDG), Mashhad, Iran, Islamic Republic of, pp. 1-6. <https://doi.org/10.1109/ICREDG54199.2022.9804556>
- [10] Errouha, M., Combe, Q., Ouanjli, N.E., Motahhir, S. (2024). A review of modern techniques for efficient control of AC motors utilized in PV water pumping system. *Irrigation Science*, 1-21. <https://doi.org/10.1007/s00271-024-00952-4>
- [11] El Mourabit, Y., Derouich, A., El Ghzizal, A., El Ouanjli, N., Zamzoum, O. (2020). Nonlinear backstepping control for PMSG wind turbine used on the real wind profile of the Dakhla-Morocco city. *International Transactions on Electrical Energy Systems*, 30(4): e12297. <https://doi.org/10.1002/2050-7038.12297>
- [12] Moulay, F., Habbati, A., Lousdad, A. (2022). The design and simulation of a photovoltaic system connected to the grid using a boost converter. *Journal Européen des Systèmes Automatisés*, 55(3): 367-375. <https://doi.org/10.18280/jesa.550309>
- [13] Mossa, M.A., Gam, O., Bianchi, N., Quynh, N.V. (2022). Enhanced control and power management for a renewable energy-based water pumping system. *IEEE Access*, 10: 36028-36056. <https://doi.org/10.1109/ACCESS.2022.3163530>
- [14] Toriki, M.B., Asy'ari, M.K., Musyafa, A. (2021). Enhanced performance of PMSG in WECS using MPPT-fuzzy sliding mode control. *Journal Européen des Systèmes Automatisés*, 54(1): 85-96. <https://doi.org/10.18280/jesa.540110>
- [15] Prince, M.K.K., Arif, M.T., Gargoom, A., Oo, A.M., Haque, M.E. (2021). Modeling, parameter measurement, and control of PMSG-based grid-connected wind energy conversion system. *Journal of Modern Power Systems and Clean Energy*, 9(5): 1054-1065. <https://doi.org/10.35833/MPCE.2020.000601>
- [16] Mehazzem, F., Reama, A. (2020). Integral backstepping control for water pumping system FED by MPPT fuzzy-logic PV source. In 2020 2nd International Conference on Smart Power & Internet Energy Systems (SPIES), Bangkok, Thailand, pp. 111-115. <https://doi.org/10.1109/SPIES48661.2020.9243002>
- [17] Veselić, B., Peruničić-Draženović, B., Milosavljevic, Č. (2008). High-performance position control of induction motor using discrete-time sliding-mode control. *IEEE Transactions on Industrial Electronics*, 55(11): 3809-3817. <https://doi.org/10.1109/TIE.2008.2006014>
- [18] Mahmood, A.S., Teke, M., Ibrahim, R.K., Hussein Ali, A., Abdulrazzaq, A.A., Kareem, M.M. (2022). Tracking the MPP of a PV system using an advanced fuzzy logic control technique. In 2022 Second International Conference on Advances in Electrical, Computing, Communication and Sustainable Technologies (ICAECT), Bhilai, India, pp. 1-7. <https://doi.org/10.1109/ICAECT54875.2022.9808009>
- [19] Mennad, M., Bentaallah, A., Djeriri, Y., Ameer, A., Bessas, A. (2024). Design of a standalone hybrid power system and optimization control with intelligent MPPT algorithms. *Journal of Polytechnic*, 27(1): 153-167. <https://doi.org/10.2339/politeknik.952553>
- [20] Mennad, M., Abderrahim, B., Youcef, D. (2022). Advanced multilayer cascade multilayer deep neural network based grid integration of hybrid PV and wind energy system. *European Journal of Electrical Engineering*, 24(1): 1-12. <https://doi.org/10.18280/ejee.240101>
- [21] Abo-Sennah, M.A., El-Dabah, M.A., & Mansour, A.E. B. (2021). Maximum power point tracking techniques for photovoltaic systems: A comparative study. *International Journal of Electrical and Computer Engineering*, 11(1): 57-73. <https://doi.org/10.11591/ijece.v11i1.pp57-73>
- [22] Abouddrar, I., El Hani, S., Heyine, M.S., Naseri, N. (2019). Dynamic modeling and robust control by adrc of grid-connected hybrid PV-wind energy conversion system. *Mathematical Problems in Engineering*, 2019(1): 8362921. <https://doi.org/10.1155/2019/8362921>
- [23] Salem, A.A., Aldin, N.A.N., Azmy, A.M., Abdellatif, W.S.E. (2021). Implementation and validation of an adaptive fuzzy logic controller for MPPT of PMSG-based wind turbines. *IEEE Access*, 9: 165690-165707. <https://doi.org/10.1109/ACCESS.2021.3134947>
- [24] Chaabane, H., Eddine, K.D., Salim, C., Djamel, H. (2021). Speed sensorless vector control of double star induction machine using sliding mode observer based Lyapunov stability. *Modelling, Measurement and Control A*, 94(1-4): 1-7. [https://doi.org/10.18280/mmc\\_a.941-401](https://doi.org/10.18280/mmc_a.941-401)
- [25] Liu, P., Hao, L. (2006). Vector control-based speed sensorless control of induction motors using sliding-mode controller. In 2006 6th World Congress on Intelligent Control and Automation, Dalian, China, pp. 1942-1946. <https://doi.org/10.1109/WCICA.2006.1712695>
- [26] El Azzaoui, M., Mahmoudi, H., Ed-Dahmani, C., Boudaraia, K. (2017). Comparing performance of PI and Sliding Mode in control of grid connected doubly fed induction generator. In 2016 International Renewable and Sustainable Energy Conference (IRSEC), Marrakech, Morocco, pp. 769-774. <https://doi.org/10.1109/IRSEC.2016.7984001>
- [27] Sebaaly, F., Vahedi, H., Kanaan, H.Y., Moubayed, N., Al-Haddad, K. (2016). Design and implementation of space vector modulation-based sliding mode control for grid-connected 3L-NPC inverter. *IEEE Transactions on Industrial Electronics*, 63(12): 7854-7863. <https://doi.org/10.1109/TIE.2016.2563381>
- [28] Rahali, H., Zeghlache, S., Benalia, L., Layadi, N. (2018). Sliding mode control based on backstepping approach for a double star induction motor (DSIM). *Advances in Modelling and Analysis C*, 73(4): 150-157. [https://doi.org/10.18280/ama\\_c.730404](https://doi.org/10.18280/ama_c.730404)

## NOMENCLATURE

$f$	frictional constant of IM, N.m.rad.sec <sup>-1</sup>
$f_g$	frictional constant of PMSG, N.m.rad.sec <sup>-1</sup>
$L_{gd}, L_{gq}$	inductances of PMSG stator in d,q frame, H

$L_s, L_r$	stator and rotor inductance of IM, H
$L_m$	mutual inductance of IM, H
$i_{gq}, i_{gd}$	components of stator current vector of PMSG d,q frame, A
$i_{sq}, i_{sd}$	components of stator current vector of IM in d,q frame, A
$J_g$	inertia torque of PMSG, Kg.m <sup>2</sup>
$J$	inertia torque of IM, Kg.m <sup>2</sup>
$R_s, R_r$	stator and rotor resistance of IM, $\Omega$
$R_g$	stator resistance of PMSG, $\Omega$
$R$	length of turbine blade, m
$T_L$	load torque of IM, N.m
$v_{gd}, v_{gq}$	components of stator voltage vector of PMSG, V
$v_{sq}, v_{sd}$	components of stator voltage vector of IM, V
$V$	wind speed, m/sec
$\omega_m$	mechanical angular speed of turbine, rad/sec
$\omega_g$	electrical speed of PMSG, rad.sec <sup>-1</sup>

$\omega_k$	rotation speed of d,q frame, rad.sec <sup>-1</sup>
$\omega$	electrical angular speed of rotor of IM, rad.sec <sup>-1</sup>

### Greek symbols

$\rho$	air density, kg/m <sup>3</sup>
$\beta$	pitch angle of blade, deg
$\Omega$	mechanical speed of IM, rad.sec <sup>-1</sup>
$\Phi_m$	permanent magnet flux, wb
$\Phi_{rq}, \Phi_{rd}$	components of rotor flux vector of IM in d,q frame, wb

### Subscripts

$P_g$	number of poles pairs for PMSG
$P$	number of poles pairs for IM